

Can a Hydroxynitrile Lyase Catalyze an Oxidative Cleavage?

Coloma, José; Hagedoorn, Peter Leon; Bento, Isabel; Hanefeld, Ulf

DOI

[10.1021/acscatal.3c02249](https://doi.org/10.1021/acscatal.3c02249)

Publication date

2023

Document Version

Final published version

Published in

ACS Catalysis

Citation (APA)

Coloma, J., Hagedoorn, P. L., Bento, I., & Hanefeld, U. (2023). Can a Hydroxynitrile Lyase Catalyze an Oxidative Cleavage? *ACS Catalysis*, 13(16), 11182-11194. <https://doi.org/10.1021/acscatal.3c02249>

Important note

To cite this publication, please use the final published version (if applicable).
Please check the document version above.

Copyright

Other than for strictly personal use, it is not permitted to download, forward or distribute the text or part of it, without the consent of the author(s) and/or copyright holder(s), unless the work is under an open content license such as Creative Commons.

Takedown policy

Please contact us and provide details if you believe this document breaches copyrights.
We will remove access to the work immediately and investigate your claim.

Can a Hydroxynitrile Lyase Catalyze an Oxidative Cleavage?

José Coloma, Peter-Leon Hagedoorn, Isabel Bento, and Ulf Hanefeld*



Cite This: ACS Catal. 2023, 13, 11182–11194



Read Online

ACCESS |



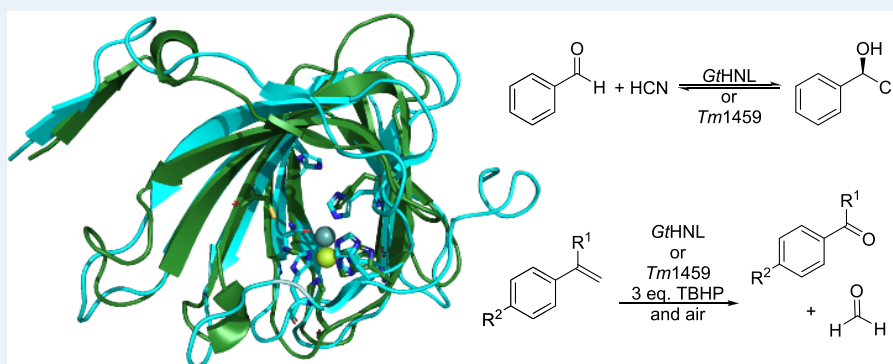
Metrics & More



Article Recommendations



Supporting Information



ABSTRACT: *Granulicella tundricola* hydroxynitrile lyase (GtHNL) is a manganese dependent cupin that catalyzes the enantioselective synthesis of cyanohydrins. The analysis of its active site shows high similarity with the active site of cupin Tm1459 from *Thermotoga maritima*, an enzyme that catalyzes the oxidative cleavage of styrene derivatives. GtHNL (GtHNL-WT) was found to catalyze the oxidative cleavage of α -methyl styrene, too. The conversion of α -methyl styrene yielded $23.6 \pm 0.8\%$ of acetophenone after 20 h. On the other hand, Tm1459 was not able to catalyze the synthesis of cyanohydrins efficiently. A low yield of *rac*-mandelonitrile was obtained from benzaldehyde and HCN using either Tm1459-WT or Tm1459-C106L, a variant more active in oxidative catalysis. On the basis of the molecular analysis of GtHNL and Tm1459 active sites, the variants GtHNL-H96A, GtHNL-H96F, and GtHNL-A40H/V42T/H96A/Q110H were produced and evaluated for improved catalytic activity toward oxidative cleavage of styrenes. The amino acid substitution H96A liberates an additional manganese coordination position and enlarges the GtHNL-WT active site cavity. Similarly, the amino acid substitution H96F liberates a coordination site as described for the GtHNL-H96A variant but without enlarging the active site space. All variants were able to catalyze the oxidative cleavage of styrene derivatives. The best results were observed using GtHNL-H96A as catalyst. It displayed a higher yield of acetophenone (42%) as compared to GtHNL-A40H/V42T/H96A/Q110H (12%) and GtHNL-H96F (11%) after 20 h of reaction time. No oxidation of Mn(II) to Mn(III) could be detected by electron paramagnetic resonance (EPR), whereas evidence for a radical mechanism is presented. Control reactions using 0.1 and 0.5 mM of MnCl₂ in the absence of enzyme showed no significant oxidation reaction.

KEYWORDS: hydroxynitrile lyase, cyanohydrin, peroxidase, ozonolysis, cupin, promiscuity, selectivity

INTRODUCTION

Two manganese containing cupins have attracted special attention as interesting biocatalysts. *Granulicella tundricola* hydroxynitrile lyase (GtHNL) catalyzes both the synthesis of cyanohydrins (Scheme 1A) and, as a promiscuous activity of all known HNLs, the nitro-aldol reaction (Henry reaction).^{1–6} Both reactions are catalyzed by the Lewis acidic Mn(II) that activates the carbonyl compound, whereas the His106 residue acts as base to deprotonate the nucleophiles (Figure 1). The cupin Tm1459 from *Thermotoga maritima* (Figure 1)⁷ has been reported to oxidatively cleave alkenes with *tert*-butyl hydroperoxide (TBHP) in the presence of oxygen from air (Scheme 1B).^{8,9} Hydrogen peroxide was not a suitable oxidation reagent, making it a rather unusual reaction in biocatalysis. Moreover, the mechanism of this reaction is unknown, but Mn(III) and a radical mechanism involving

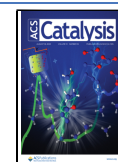
oxygen and TBHP have been suggested. Redox chemistry of Mn typically involves oxidized Mn species such as Mn(III) or Mn(IV), but limited or no evidence for this is currently available for Tm1459.^{8,9}

The cupin superfamily has a conserved beta-barrel fold and constitutes a versatile scaffold in biocatalysis.^{10–12} With many different divalent metal cations such as Fe²⁺, Cu²⁺, Zn²⁺, Co²⁺, Ni²⁺, or Mn²⁺ complexed by between three and five amino acids of the cupin, a wide range of reactions can be catalyzed.

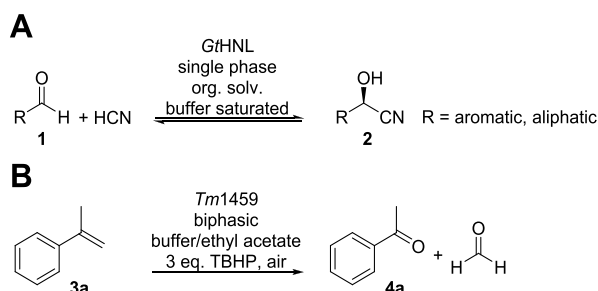
Received: May 17, 2023

Revised: July 10, 2023

Published: August 9, 2023



Scheme 1. The Mn(II) Containing Cupins *GtHNL* and *Tm1459* Are Versatile Catalysts^a



^a(A) *GtHNL* catalyzes the formation of *R*-cyanohydrins. (B) *Tm1459* catalyzes the oxidative cleavage of styrene derivatives, equivalent to the ozonolysis reaction.

When comparing *GtHNL* and *Tm1459*, the striking similarity of the *GtHNL* and *Tm1459* active sites (Figure 1 and Figure S1) raises the question about their potential promiscuous activity toward the oxidative cleavage of styrenes (3) and the synthesis of cyanohydrins (2), respectively. This is despite the fact that their overall sequence identity (28%) and similarity (35%) are moderate (Figure S2). The *GtHNL* active site has only a single coordination site of the Mn(II) available for the substrate to bind and contains a base (His106), whereas *Tm1459* has two coordination sites at Mn(II) available and therefore more space around the metal cofactor but no basic residues nearby. Cys106 is not essential for the activity of *Tm1459*; the C106L variant displayed improved alkene cleavage activity.^{8,9} Herein, the interchangeability of *GtHNL* and *Tm1459* catalysis is probed by studying their promiscuous activities, i.e., the HNL activity of *Tm1459* and the alkene oxidative cleavage activity of *GtHNL*. Electron paramagnetic resonance (EPR), structural, and biocatalytic studies were performed to cast light on the mechanism of the oxidative cleavage reaction.

RESULTS AND DISCUSSION

***Tm1459* Exhibits Moderate and Unselective HNL Activity.** The potential promiscuous catalytic activity of *Tm1459* and *GtHNL* toward the synthesis of cyanohydrins and the oxidative cleavage of styrenes, respectively, was assessed. *Tm1459* and *Tm1459*-C106L, a more active variant

for the oxidative cleavage of styrenes, were evaluated for the conversion of benzaldehyde (1a) and HCN to mandelonitrile (2a; Scheme 2A). For direct comparison, optimal conditions for *GtHNL* were employed.³ Under these conditions, *GtHNL*-A40H/V42T/Q110H gave complete conversion of 1a to *R*-2a after 4 h of reaction time with an *ee* \geq 99%. Both variants, *Tm1459* and *Tm1459*-C106L, were immobilized on Celite-R633, and methyl *tert* butyl ether (MTBE) saturated with sodium acetate buffer pH 4 was used as the reaction medium.³ *Tm1459* and *Tm1459*-C106L yielded *rac*-2a (31 \pm 0.17 and 43 \pm 0.14%, respectively) after 24 h of reaction time. As the chemical background reaction is known to lead to misassignments of HNL activity, blank reactions were performed.¹³ In this case, the reaction with just the enzyme carrier but without enzyme yielded *rac*-2a (23 \pm 0.33%). These results indicate that the HNL activity for the *Tm1459* cupins is modest and unselective. The Celite-R633 immobilized *Tm1459*-C106L was also evaluated in a biphasic system using the conditions reported earlier for the oxidative styrene cleavage reaction. A total of 21 \pm 0.3% of *rac*-2a was formed after 2 h compared to 14 \pm 0.66% for the blank reaction. The potential *Tm1459* catalyzed synthesis of 2a was not further investigated given the low yields and lack of selectivity displayed by either *Tm1459* or *Tm1459*-C106L and the large number of selective HNLs available.^{14,15} The lack of activity and enantioselectivity cannot be ascribed to the absence of a base such as His106 in *GtHNL*, as work with copper variants of *Tm1459* has demonstrated successful deprotonation of nitroalkanes and methyl acetoacetate.^{16–18}

***GtHNL* Catalyzed the Oxidative Cleavage of Styrenes Using TBHP.** The initial oxidative cleavage reactions were performed under conditions earlier optimized for *Tm1459*.^{8,9} To our delight, *GtHNL* was able to catalyze the oxidative cleavage of α -methyl styrene (3a) with a yield of acetophenone (4a) of 23.6 \pm 0.8% after 20 h of reaction time. Similarly, *GtHNL*-A40H/V42T/Q110H (*GtHNL*-3V), a more active variant for the synthesis of cyanohydrins,^{2,3} displayed a yield of 4a of 17.8 \pm 0.4% after equal reaction time. These enzyme catalyzed reactions were clearly distinguishable from control reactions either using 0.1 mM MnCl₂ (4.1 \pm 0.65% yield) or without MnCl₂ (1.4 \pm 0.01% yield). These preliminary findings showed that only one coordination position on the Mn(II) in the *GtHNL* active site is needed for substrate binding. This is in line with the observation that oxidative

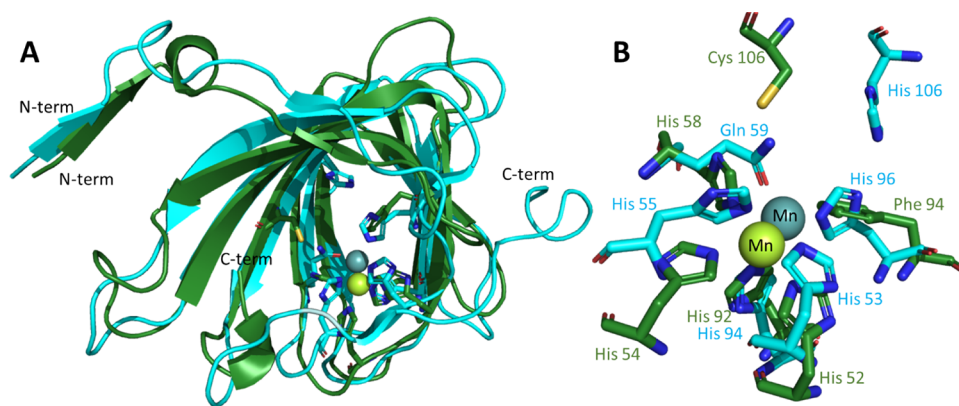


Figure 1. (A) Superimposition of *GtHNL* (PDB code: 4BIF) in blue with Mn(II) in gray coordinated by four histidines and one glutamine and *Tm1459* (PDB code: 1VJ2) in green with Mn(II) in lime coordinated by four histidines. (B) Superimposition of the key residues in the active sites and the metal cofactor of *GtHNL* and *Tm1459*. The images were created using the PyMOL Molecular Graphics System.

Scheme 2. (A) *Tm1459* Immobilized on Celite R-633 in Buffer Saturated MTBE or Biphasic Mixture for the Synthesis of Mandelonitrile (**2a**). (B) *GtHNL*-Catalyzed Oxidative Cleavage of Styrene Derivatives (**3a–h**)

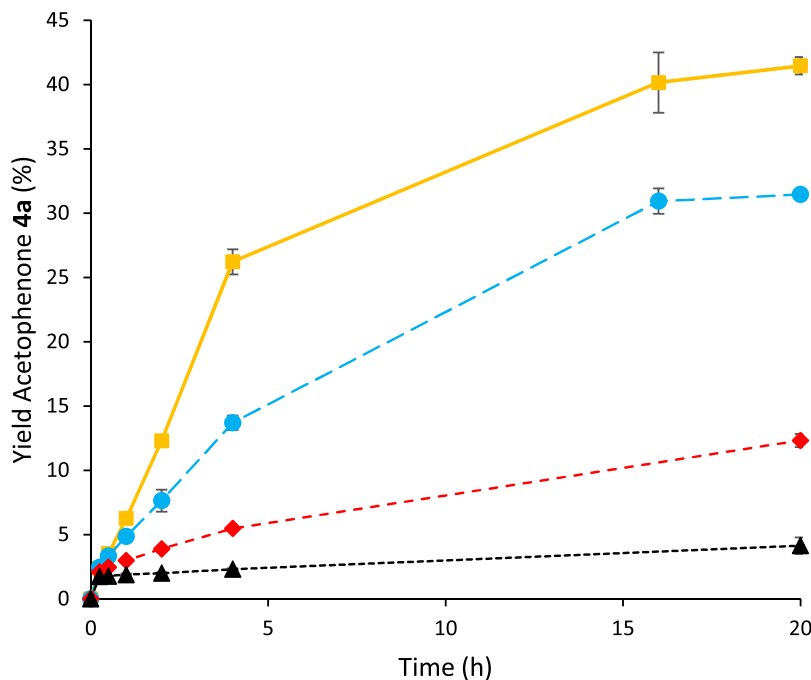
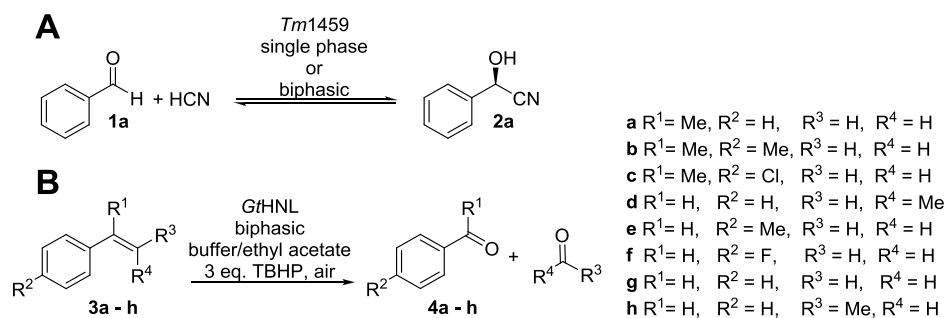


Figure 2. Oxidative cleavage of α -methyl styrene catalyzed by *GtHNL*. Reaction conditions: 50 mM α -methyl styrene (**3a**) in ethyl acetate, 150 mM TBHP, 2 mg *GtHNL*-H96A or *GtHNL*-A40H/V42T/H96A/Q110H, 50 mM sodium phosphate buffer pH 7, 30 °C, and 1000 rpm. Reactions were not quenched with sodium bisulfite. Reaction volume: 1 mL. Orange squares and solid line (■): *GtHNL*-H96A overexpressed with 0.5 mM MnCl_2 ; blue dots and long dashed line (●): *GtHNL*-H96A overexpressed with 0.1 mM MnCl_2 ; red diamonds and dashed line (◆): *GtHNL*-4V overexpressed with 0.1 mM MnCl_2 ; black triangles and dotted line (▲): control reaction 0.1 mM MnCl_2 . All experiments were performed in duplicate ($n = 2$). The ratio of the organic/aqueous phase was 1:9.

reactions catalyzed by Mn typically proceed via an oxidized Mn species and that Mn can also be hepta-coordinated, as proposed for superoxide dismutase (SOD).^{19–21} On the other hand, an additional free coordination position (as in the *Tm1459* active site) might provide a wider active site, a more polarized charged metal site, and consequently a more Lewis acidic manganese.^{22,23}

The His96 was substituted for Ala in *GtHNL* and *GtHNL*-3V. Importantly, this amino acid substitution should not affect the incorporation of manganese during the enzyme overexpression.¹ In analogy with *Tm1459*, the amino acid substitution H96F was also introduced into *GtHNL*-WT (Figure 1B). **3a** was used as model substrate. Higher yields were achieved by *GtHNL*-H96A. This variant was able to catalyze the oxidative cleavage of **3a** to acetophenone (**4a**) with a yield of $31.8 \pm 0.7\%$ in 16 h, comparable to the conversion (30%) that has been reported for *Tm1459* under similar reaction conditions.^{8,9} In these earlier reports, sodium

bisulfite had been employed to quench the reaction. This is however known to form bisulfite adducts with aldehydes and ketones. Indeed, a lower yield of **4a** (18.8%) was observed if a small amount of sodium bisulfite (circa 50–70 mg) was used to stop the reaction, as reported earlier.^{8,9} Therefore, no sodium bisulfite quenching was applied, but instead, a rapid workup ensured that the reaction was halted completely. *GtHNL*-A40H/V42T/H96A/Q110H (*GtHNL*-4V) and *GtHNL*-H96F reached only 12 and 11% yield of **4a** (without bisulfite quenching), respectively.

The improved catalytic activity of *GtHNL*-H96A compared to *GtHNL* and *GtHNL*-H96F might be explained by the more accessible metal cofactor. The bulky histidine and phenylalanine residues potentially block part of the active site. Larger active sites have been reported as one of the mechanisms that enable catalytic promiscuity because the substrates can adopt different orientations within the active site.²⁴

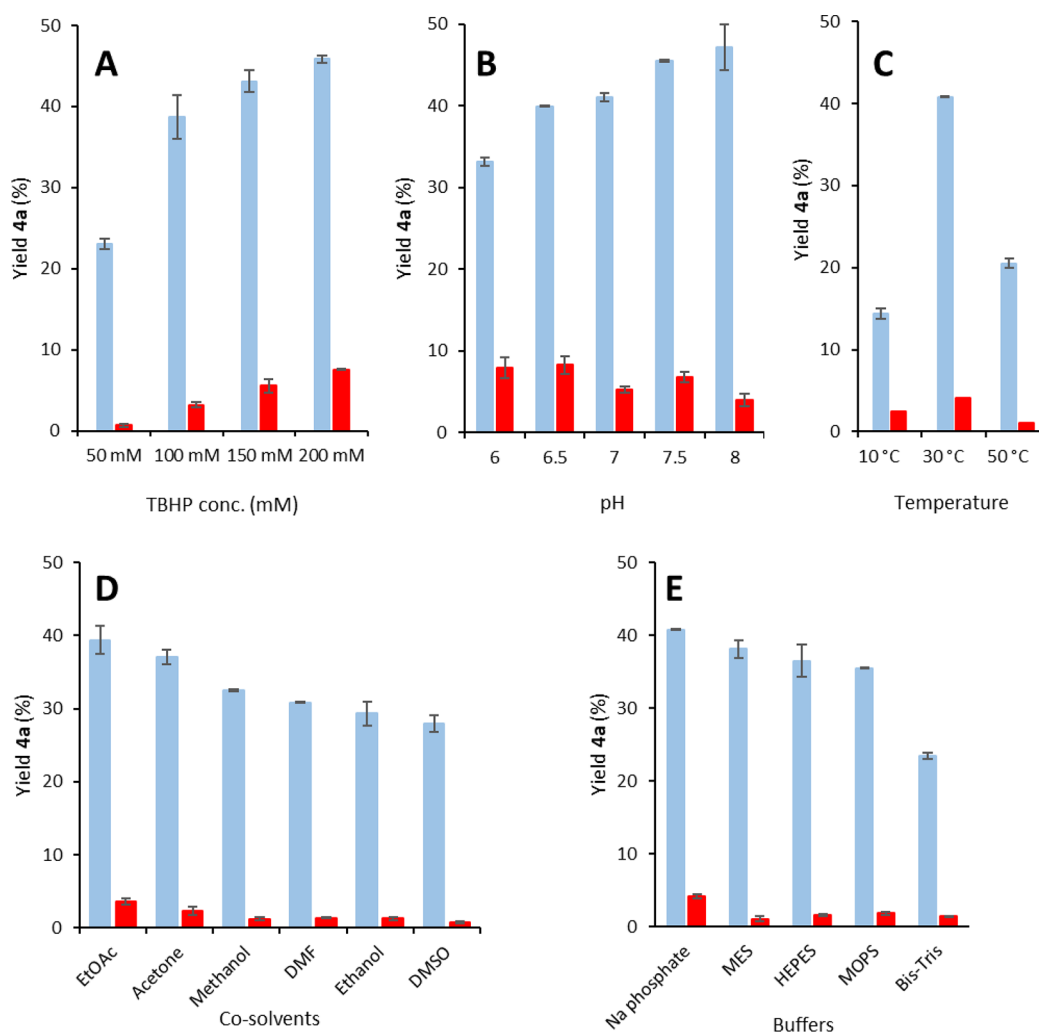


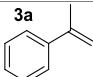
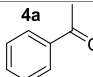
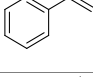
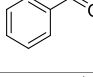
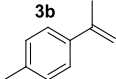
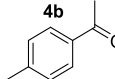
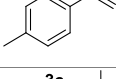
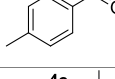
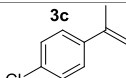
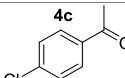
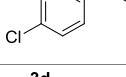
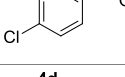
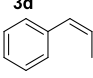
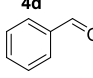
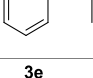
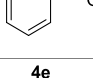
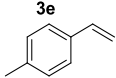
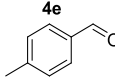
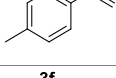
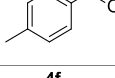
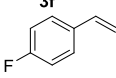
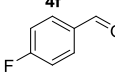
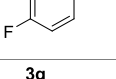
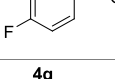
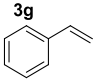
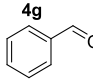
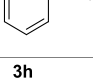
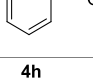
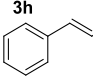
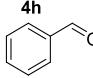
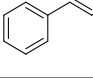
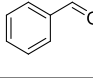
Figure 3. Reaction optimization for the oxidative cleavage of **3a** catalyzed by *GtHNL-H96A*. (A) Influence of different TBHP concentrations. Reaction conditions: 50 mM substrate in ethyl acetate, 50–200 mM TBHP, 2 mg *GtHNL-H96A*, 50 mM sodium phosphate buffer pH 7, 30 °C, and 20 h. (B) Influence of different pH values. Reaction conditions: 50 mM substrate in ethyl acetate, 150 mM TBHP, 2 mg *GtHNL-H96A*, 50 mM sodium phosphate buffer pH 6–8, 30 °C, and 20 h. (C) Influence of temperature. Reaction conditions: 50 mM substrate in ethyl acetate, 150 mM TBHP, 2 mg *GtHNL-H96A*, 50 mM sodium phosphate buffer pH 7, 10–50 °C, and 20 h. (D) Influence of different co-solvents. Reaction conditions: 50 mM substrate in different co-solvents, 150 mM TBHP, 2 mg *GtHNL-H96A*, 50 mM sodium phosphate buffer pH 7, 30 °C, and 20 h. The ratio of organic/aqueous phase was 1:9. (E) Influence of different buffers. Reaction conditions: 50 mM substrate in ethyl acetate, 150 mM TBHP, 2 mg *GtHNL-H96A*, 50 mM sodium phosphate, MES, HEPES, MOPS or Bis-Tris buffers pH 7, 30 °C, and 20 h. All enzymatic reactions were performed with 2 mg *GtHNL-H96A* overexpressed in the presence of 0.5 mM MnCl_2 . Light blue bars are enzymatic reactions. Red bars are control reactions performed with 0.5 mM MnCl_2 . All reactions were performed in duplicate in 1 mL reaction volume and shaken at 1000 rpm without quenching at the end of the reaction time.

GtHNL-H96A and *GtHNL-4V* were expressed in a culture medium containing 0.1 mM MnCl_2 . Nonetheless, ICP-OES analysis revealed a different Mn(II) loading of 9.3 and 25% for *GtHNL-H96A* and *GtHNL-4V*, respectively. Because manganese is essential for the catalytic activity of *GtHNL* for the synthesis of cyanohydrins,^{1,4} MnCl_2 supplementation (from 0.1 to 1 mM) during *GtHNL-H96A* overexpression was investigated to improve the catalytic activity of *GtHNL-H96A*. Higher yields of **4a** were achieved when *GtHNL-H96A* was obtained from cells in which the enzyme was overexpressed in the presence of 0.5 mM MnCl_2 (Figure 2 and Figure S3). In addition, the *in vitro* incubation of *GtHNL-H96A* (obtained from cells in which the enzyme was overexpressed in the presence of 0.1 mM MnCl_2) with 10 molar equiv of MnCl_2 for 5 h allowed higher manganese loadings (30%). Consequently, the product yield increased slightly from 31.5 to 35% **4a**

(Figure S3, red bar). Similarly, *GtHNL-4V* was incubated with 10 molar equiv of MnCl_2 but without significant improvement of **4a** yield (15% after 20 h; the final Mn(II) concentration was not determined). Overall, *GtHNL-H96A* proved to be a better variant for the oxidative cleavage of **3a**, although the manganese loading was lower than in *GtHNL-4V*. In all cases, the enzymatic reactions are clearly distinguishable from the control reaction (Figure 2). Therefore, the variant *GtHNL-H96A* produced in the presence of 0.5 mM MnCl_2 with 0.03 U/mg, comparable to earlier work,⁸ was chosen for further work.

Optimal *GtHNL-H96A* Catalyzed Cleavage Conditions of α -Methyl Styrene. The reaction was optimized by evaluating TBHP concentration, pH value, temperature, co-solvents, and buffer composition (Figure 3). A significantly higher yield of **4a** was reached at TBHP concentrations above

Table 1. Oxidative Cleavage of Styrene Derivatives Catalyzed by *GtHNL-H96A*^a

Reaction	Substrate	Product	Substrate Conversion (%) ^b	Product Yield (%) ^c
<i>GtHNL-H96A</i>			70.7 ± 3.4	37.7 ± 0.8
Control			32.8 ± 0.5	3.9 ± 0.1
<i>GtHNL-H96A</i>			74.3 ± 0.4	31.8 ± 0.7
Control			23.6 ± 1.7	1.3 ± 0.1
<i>GtHNL-H96A</i>			64.9 ± 1.9	37.1 ± 0.3
Control			21.3 ± 0.2	8.6 ± 0.2
<i>GtHNL-H96A</i>			53.8 ± 7.0	12.3 ± 2
Control			38.2 ± 0.8	0
<i>GtHNL-H96A</i>			59.3 ± 3.6	24.4 ± 1.3
Control			30.7 ± 2.8	3.1 ± 0.1
<i>GtHNL-H96A</i>			65.6 ± 7.3	25.6 ± 2.5
Control			38.5 ± 7.9	2.3 ± 0.1
<i>GtHNL-H96A</i>			61.4 ± 5.2	26.7 ± 1.1
Control			40.4 ± 5.0	1.1 ± 0.09
<i>GtHNL-H96A</i>			61.4 ± 3.5	25.9 ± 0.6
Control			27.4 ± 0.4	0

^aReaction conditions: 50 mM substrate, 150 mM TBHP, 2 mg *GtHNL-H96A*, 50 mM sodium phosphate buffer pH 7, 30 °C, and 1000 rpm. Control reactions were performed with 0.5 mM MnCl₂. ^bBased on reacted substrate. ^cBased on the product concentration relative to the initial substrate concentration. Reaction time: 16 h. Reaction volume: 1 mL. All the reactions were NOT quenched with sodium bisulfite at the end of the reaction time. The enzyme was overexpressed in the presence of 0.5 mM MnCl₂. The ratio of the organic/aqueous phase was 1:9. All experiments were performed in duplicate (*n* = 2).

50 mM, i.e., an excess of TBHP. Additionally, the chemical background reaction was slightly accelerated (Figure 3A). *GtHNL* did not catalyze the oxidative cleavage of styrenes in the absence of TBHP. When the reaction was performed in the absence of oxygen, the yield of **4a** decreased to 6.75%. The decomposition of TBHP into alkoxy radicals and molecular oxygen during the Mn catalytic cycle^{25,26} may result in a low oxygen concentration persisting even under anaerobic conditions. This can explain why even without initial oxygen, the reaction did proceed to some extent. This suggests that both TBHP and oxygen are important for the *GtHNL* catalyzed oxidative cleavage of styrene derivatives, as had earlier been found for *Tm1459*.^{8,9} At the same time, the role of oxygen is not clear.

GtHNL-H96A displayed a higher yield of **4a** at slightly basic pH values of 7–8 (Figure 3B). An earlier report showed that *GtHNL* is active and more stereoselective at low temperatures for the synthesis of (*R*)-mandelonitrile (**2a**).^{2,3} On the other hand, during preliminary experiments, *GtHNL-3V* displayed a high thermostability. For this reason, the effect of different temperatures (10, 30, and 50 °C) was evaluated. A higher yield of **4a** was observed at 30 °C (Figure 3C). The decrease in conversion observed at 50 °C could be explained by either the

degradation or evaporation of the substrates or product at this temperature. Indeed, the boiling point of TBHP is 38 °C. Additionally, organic peroxides are known as highly flammable, extremely reactive, and toxic. The temperature in reactions with TBHP must not exceed 55.6 °C to ensure safe reaction conditions.²⁷ The mass balance analysis of the reactions showed a good mass balance only for the reactions performed at 10 °C, suggesting that higher temperatures cause loss or degradation of substrates or product (Table S1). This together with safety considerations led to the choice of 30 °C as reaction temperature.

The influence of five different co-solvents on the synthesis of product **4a** was investigated. The reactions were performed with 5% (v/v) of co-solvent. Ethyl acetate and acetone with a log *P* of 0.71 and −0.24, respectively, displayed the highest yields of **4a** (Figure 3D), but no clear relation between the solvent log *P* and yield was observed. Special attention must be given when TBHP is mixed with acetone as an explosive mixture might result. When TBHP is mixed with organic solvents under acidic conditions, a violent decomposition may occur. As mentioned above, the temperature must not exceed 55.6 °C for safety reasons.²⁷ Buffers (50 mM) in the same p*K*_a range (p*K*_a ~ 7) were used to evaluate their influence on the

Table 2. *GtHNL* and *Tm1459* Catalyzed Reactions for the Synthesis of Mandelonitrile **2a** or the Oxidative Cleavage of α -Methyl Styrene **3a**^a

Catalyst	Mandelonitrile synthesis		Oxidative cleavage of α -methyl styrene
	Activity	Selectivity	
<i>GtHNL</i> -WT	Modest ^b	Modest ^b	Low ^c
<i>GtHNL</i> -A40H/V42T/Q110H	High ^d	High ^d	Low ^e
<i>GtHNL</i> -H96A	Modest ^f	Low ^g	Modest ^h
<i>GtHNL</i> -H96F	High ⁱ	Low ^j	Low ^k
<i>GtHNL</i> -A40H/V42T/H96A/Q110H	High ^l	High ^l	Low ^m
<i>Tm1459</i> -WT	Modest ⁿ	Low ^o	Modest ^p
<i>Tm1459</i> -C106L	Modest ^q	Low ^r	High ^s

^aFor the cyanohydrin formation activity: high >80% (140 U/mg),² modest 80–30%, and low <30%; selectivity: high >90%, modest 90–70%, and low <70%. For the oxidative cleavage activity: high >50% (0.03 U/mg), modest 50–30%, and low <30%. ^b80% conversion and 90% ee after 6 h of reaction time. ^c23.6% conversion after 20 h. ^d>99% conversion and >99% ee after 4 h of reaction time. ^e17.8% conversion after 20 h of reaction time. ^f47% conversion after 4 h of reaction time. ^g19% ee after 4 h of reaction time. ^h41% conversion after 20 h of reaction time. ⁱ97% conversion after 4 h of reaction time. ^jRacemic after 4 h of reaction time. ^k11% conversion after 20 h of reaction time. ^l98% conversion and 98% ee after 4 h of reaction time. ^m12% conversion after 20 h of reaction time. ⁿ31% conversion after 24 h of reaction time. ^oRacemic after 24 h of reaction time. ^p30% conversion after 20 h of reaction time. ^q43% conversion after 24 h of reaction time. ^rRacemic after 24 h of reaction time. ^s60% conversion after 20 h of reaction time.⁹

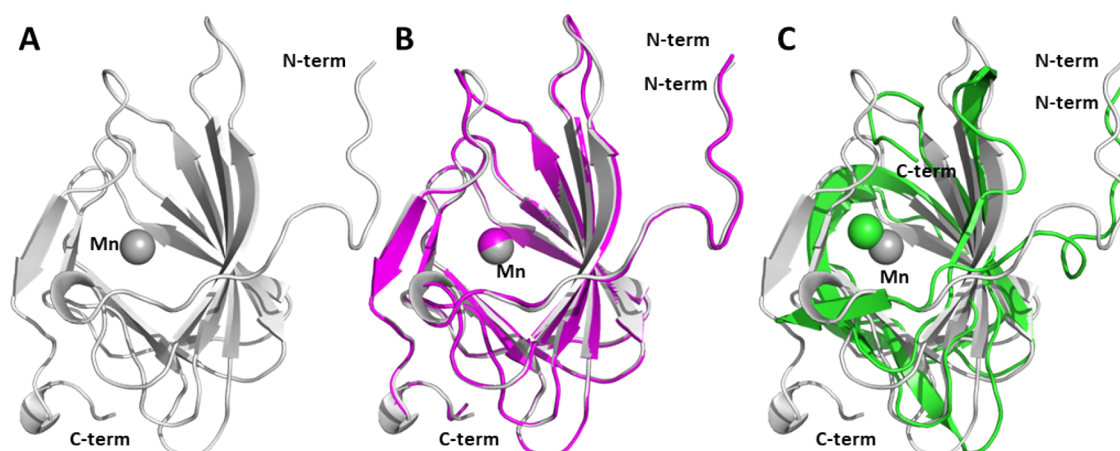


Figure 4. Crystal structure of *GtHNL*-H96A (PDB ID: 8OZ8). (A) *GtHNL*-H96A monomer displaying the cupin beta-barrel fold. (B) Superimposition of *GtHNL*-H96A (gray) and *GtHNL*-WT (PDB code: 4BIF, magenta) with an RMSD of 0.4 Å for 131 Ca atoms. (C) Superimposition of *GtHNL*-H96A (gray) and *Tm1459* (PDB code: 1VJ2; green) with an RMSD of 1.8 Å for 109 Ca atoms.

catalytic activity of *GtHNL*-H96A (Figure 3E). The highest yield was reached with sodium phosphate buffer pH 7, and an important decrease in yield was observed with Bis–Tris buffer as the reaction medium, which may be due to the metal chelating properties of that buffer.^{28,29}

***GtHNL*-H96A Has a Broad Substrate Scope toward Substituted Styrene Derivatives.** Having established the best reaction conditions for the *GtHNL*-H96A catalyzed oxidative cleavage of **3a**, the substrate scope was evaluated toward different substituted styrene derivatives. *GtHNL*-H96A was active and chemoselective for the oxidative cleavage. Control reactions with 0.5 mM of MnCl₂ in the absence of enzyme showed significantly lower conversions (Table 1). The oxidative cleavage product corresponds to around 50% of the reacted substrate for most of the styrenes evaluated and less than 10% for the control reactions. *GtHNL*-H96A showed a similar product yield for substrate **3c** when compared to an earlier report using *Tm1459* as catalyst. For substrates **3a**, **3e**, **3g**, and **3h**, *GtHNL*-H96A gave almost twice the product yield

as compared to *Tm1459*. However, *Tm1459* displayed a selectivity >95% for most of the substrates evaluated.⁸ For variants *Tm1459*-C106L and *Tm1459*-C106Q, a conversion of 60% using **3a** as substrate was reported.⁹

The presence of a methyl group at the α -position of the styrene double bond (**3a**, **3b**, and **3c**) favored the oxidative cleavage. The corresponding ketones were formed in yields of 37.7, 31.8, and 37.1%, respectively, after 16 h of reaction time and identified by GC–MS (Figure S4). The absence of a methyl group on the double bond at the α position (**3d**, **3e**, **3f**, **3g**, **3h**) including a shift to the β -position (**3d**, **3h**) resulted in a drastic decrease in yield. Electron-donating (**3b**, **3e**) or -withdrawing groups (**3c**, **3f**) on the phenyl ring did not further improve the yields. Overall, the presence of a methyl group at the α -position of the double bond exerted the highest influence on the yields achieved. This suggests radical formation as part of the mechanism because **3a–c** form more stable benzylic radicals than **3d–h**, as will be discussed below. Table 1 shows that both aromatic aldehydes and

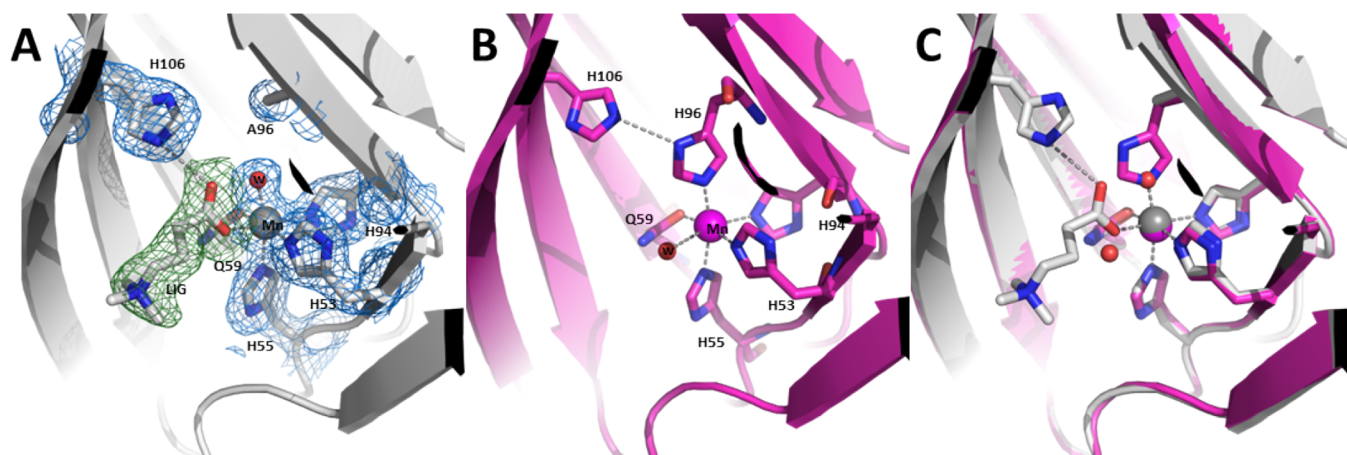


Figure 5. Detail of the Mn ion (A) *GtHNL*-H96A variant (PDB ID: 8OZ8) showing a water molecule occupying the coordination position freed by the H96 side chain and a ligand molecule occupying the other vacant coordination position. Electron density maps $2mFo - DFc$ (in blue) and $mFo - DFc$ (in green) contoured at 1.0 and 3.0 sigma levels, respectively. (B) *GtHNL* Mn ion (PDB code: 4BIF) with the free coordination position occupied by a water molecule. (C) Superimposition of *GtHNL*-H96A (gray) and *GtHNL* (magenta).

ketones are accessible. *GtHNL*-H96A did not catalyze the oxidative cleavage of aliphatic alkenes.

Synthesis reactions of (*R*)-mandelonitrile (**2a**) were performed to evaluate if *GtHNL*-H96A, *GtHNL*-H96F, and *GtHNL*-4V sacrifice their natural cyanogenesis activity for a peroxidase-like activity or if the oxidative cleavage activity is added to its natural activity. The three variants were found to maintain their natural activity. *GtHNL*-H96A displayed a conversion of $47 \pm 0.008\%$ ($ee = 19\%$). *GtHNL*-4V and *GtHNL*-H96F showed almost full conversion (98%) but partially low enantioselectivity; the ee 's of the products were 98 and 2.6%, respectively, which correspond to enantioselectivities of 99 and 1.05, respectively (Figure S5). The excellent enantioselectivity observed for *GtHNL*-4V is not surprising because its progenitor *GtHNL*-3V is an excellent enzyme for the synthesis of chiral cyanohydrins.^{2,3} The improved deprotonation of hydrogen cyanide facilitated by additional histidines, the narrower active site, and more tightly bound manganese can explain this result. On the other hand, *GtHNL*-H96F with a more congested active site loses enantioselectivity completely.

A brief summary of the ability of *GtHNL* and *Tm1459* to catalyze either the synthesis of mandelonitrile (**2a**) or the oxidative cleavage of α -methyl styrene (**3a**) is shown in Table 2.

***GtHNL*-H96A Crystal Structure.** The crystal structure of the *GtHNL*-H96A variant shows the same fold observed for *GtHNL* (PDB code: 4BIF; Figures 1 and 4). Each monomer displays the characteristic cupin jelly-roll fold, and the Mn ion is located at the base of the beta-barrel (Figure S6A). A domain-swapped dimer is formed when the *N*-terminal beta-strand of one monomer packs against the eighth beta-strand of the neighboring monomer (Figure S6B). The asymmetric unit includes four *GtHNL*-H96A monomers, comprising one domain-swapped dimer and two additional monomers (Figure S6C; average RMSD of 0.25 Å for 130 C α atoms between monomers). The functional homo-tetramer consists of two domain-swapped dimers, with the second domain-swapped dimer rotated approximately 90° compared to the first one (Figure S6D). The homo-tetramer corresponds to the entity observed for the wild-type *GtHNL* (PDB code: 4BIF), and it is also the oligomeric form found in the solution for *GtHNL*-

H96A (confirmed by SEC-MALS measurement; results not shown). At the base of the active cavity, a manganese ion was modeled and refined to an occupancy of 0.8 in all four monomers. The metal ion shows octahedral coordination and is coordinated by four of the conserved five residues (H53, H55, Q59, H94), a water molecule, and a ligand molecule. The residues are arranged in a square planar manner and located at an average distance of 2.2 Å from the metal ion. Extra positive electron density (difference electron density maps ($mFo - DFc$) at the 3.0 sigma level (Figure 5A)), which could account for more than just a water molecule, was observed in the neighborhood of the manganese ion from the beginning of the refinement. Initially, the components of the crystallization solution (KBr, Bis-Tris buffer, NaCl, PEG 2000 MME, sodium citrate) were considered putative ligands, but none of them could justify the electron density. 4-Trimethylaminobutanoic acid, part of the *E. coli* metabolome (<https://ecmdb.ca/compounds/M2MDB001736>),³⁰ was modeled as a putative ligand, with its oxo-atom at an average coordinating distance of 2.2 Å of Mn, and refined with the same occupancy observed for the metal ion (0.8) (Figure 5A). This ligand molecule binds the Mn ion where a water molecule is observed in *GtHNL* (PDB code: 4BIF, Figure 5B). The ligand moiety is positioned co-planar with H94, and the coordination site that was liberated by the mutation (H96A) is occupied by a water molecule (Figure 5). Superimposition of the *GtHNL*-H96A with *GtHNL* clearly shows that this type of ligand cannot bind to *GtHNL* as it would clash with the H96 side chain (Figure 5C).

On the other hand, this and similar ligand moieties would fit into the binding cavity of *Tm1459* (PDB code: 1VJ2), which has two free coordination positions occupied by water molecules (Figures 1 and 6B) and has been shown to oxidatively cleave styrene derivatives.^{8,9} The mutation introduced into *GtHNL* giving variant *GtHNL*-H96A increases the accessible area of the Mn ion to values comparable to the ones observed for *Tm1459* (Table S4). While increasing the accessibility of the metal, it does not induce a change in the location of the Mn ion to a position closer to the one found for *Tm1459*. Although both Mn ions are coordinated by four enzyme residues, in *GtHNL*-H96A, it adopts the same position as observed for *GtHNL* (Figure 6).

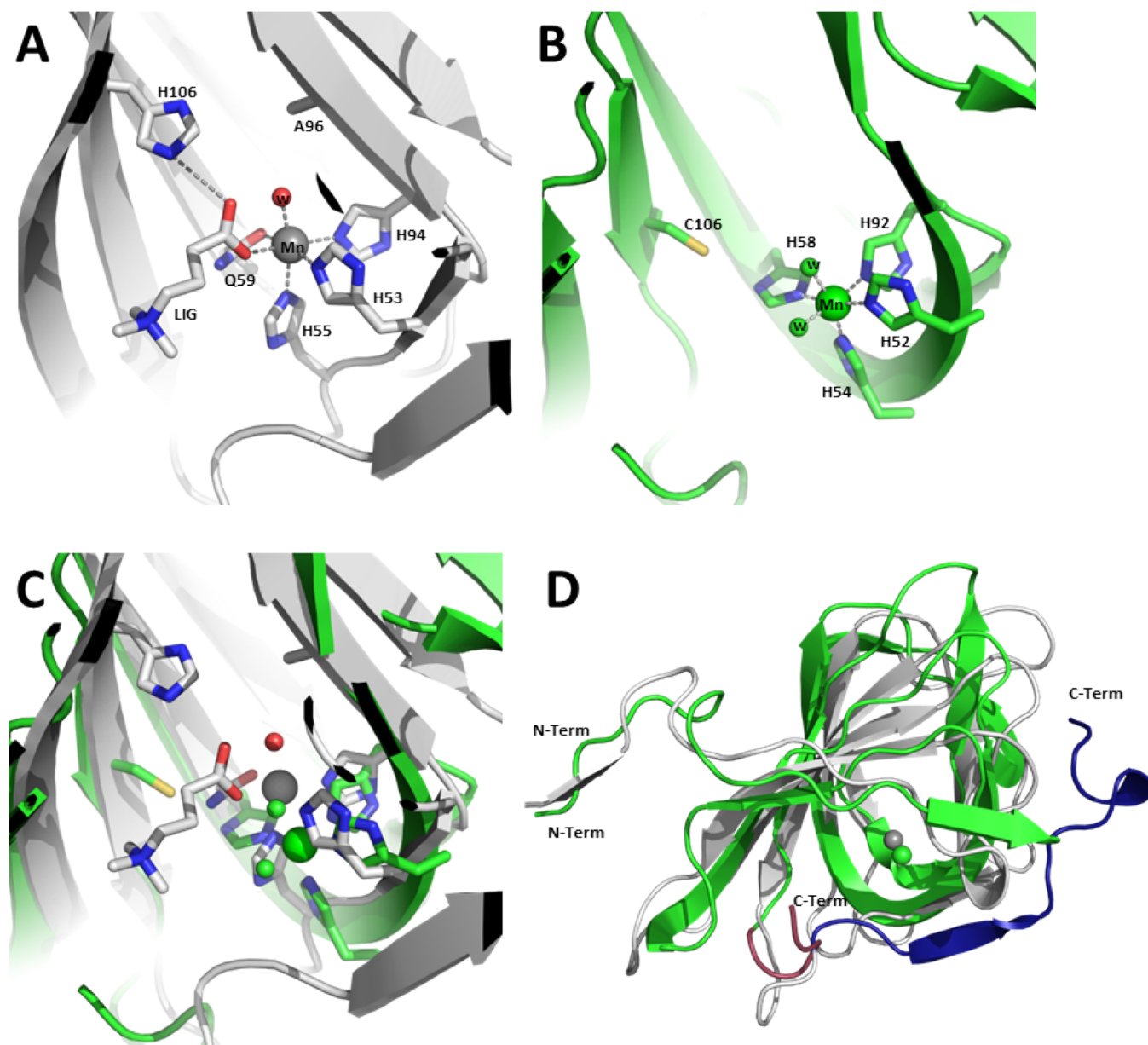


Figure 6. Detail of the Mn ion (A) *GtHNL*-H96A variant (PDB ID: 8OZ8). (B) *Tm1459* Mn ion (PDB code: 1VJ2, green) with two coordination positions occupied by water molecules. (C) Superimposition of *GtHNL*-H96A (gray) and *Tm1459* (green). (D) Superimposition of *GtHNL*-H96A (gray) and *Tm1459* (green) highlighting the location of the C-terminus. *Tm1459* C-term residues 111:114 are colored in red, and *GtHNL*-H96A C-term residues 117:131 are colored in dark blue.

The different C-termini of *GtHNL* (131 residues) and *Tm1459* (114 residues) (Figure 6D, Figure S7) could influence the coordinating residues and, consequently, the location of the Mn in *GtHNL* and *Tm1459*. Indeed, the superimposition of *GtHNL*-H96A with another cupin from *Thermotoga maritima* MSB8 (*Tm1010*-WT) (PDB code: 2F4P), with a sequence of 135 residues long, shows that all active site residues are located in positions that overlap the ones found for *GtHNL*-H96A and not for *Tm1459* (Figure S7). Although *Tm1010* lacks the metal in the active site (Figure S7), an extra beta-strand is added to the cupin beta-barrel in the C-terminus (Figure S7), as equally observed for *GtHNL*-H96A, introducing more interactions between the residues and constraining their location.

Overall, the *GtHNL*-H96A crystal structure clearly shows that the changes observed in the configuration of the Mn ion

increase the accessibility of the metal and of the active cavity, consequently enabling an improved oxidative cleavage activity, underpinning the results obtained for the oxidative cleavage of α -methyl styrenes **3** (Tables 1 and 2).

Reaction Mechanism. It was reported that Mn(III) is the most likely active species for the oxidative cleavage of alkenes catalyzed by *Tm1459*.⁸ This would potentially support a radical mechanism for the *GtHNL* catalyzed oxidative cleavage of styrenes (**3**), too.⁹ Previous electron paramagnetic resonance (EPR) studies showed that Mn(II) is the active species in the regular *GtHNL* catalyzed reaction and plays a crucial role as Lewis acid for the synthesis of chiral cyanohydrins.⁴ Therefore, the nature of manganese under the influence of TBHP as oxidant during the oxidative cleavage of **3a** was explored employing EPR. Figure 7A shows the EPR spectra of *GtHNL*-H96A before and after the addition of TBHP and **3a** measured

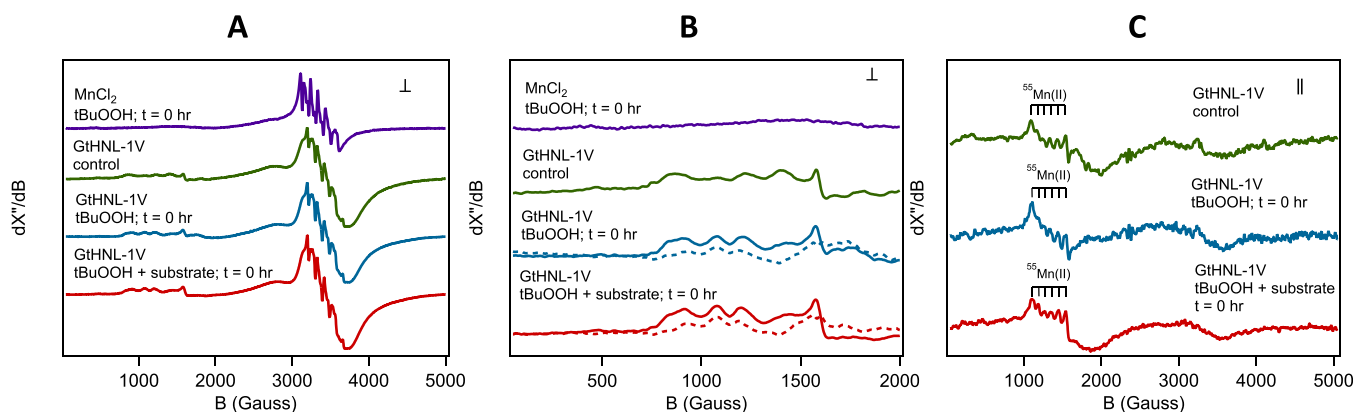


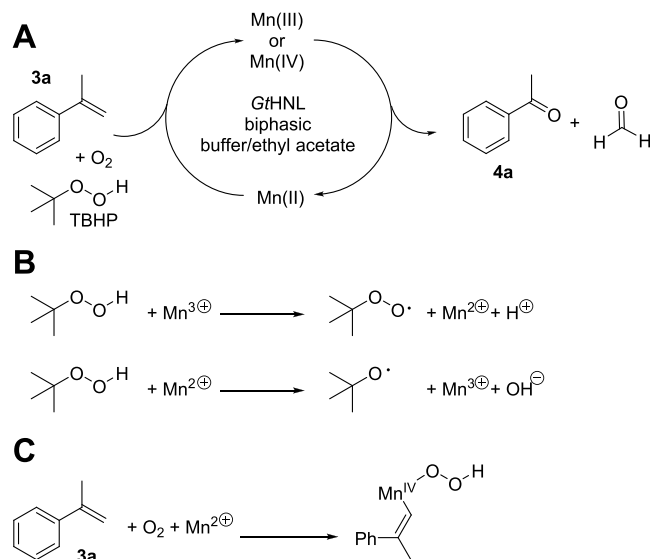
Figure 7. EPR spectra of GtHNL-H96A. (A) Perpendicular mode and (B) perpendicular mode with field range between 0 and 2000 G. Dotted lines give the difference spectrum with the control sample (without TBHP) and thereby represent the putative Mn(IV) signal and (C) parallel mode. EPR conditions: microwave frequency 9.624 GHz (perpendicular mode), 9.295 (parallel mode); microwave power 20 mW; modulation frequency 100 kHz; modulation amplitude 10 G; and temperature 12.5 K. Each spectrum was averaged four times (perpendicular mode) or nine times (parallel mode).

in perpendicular mode. Additional low field signals appear after addition of the oxidant, which we putatively attribute to Mn(IV) ($S = 3/2$). However, the Mn(IV) and Mn(II) ($S = 5/2$) signals overlap and are difficult to distinguish. A control reaction using MnCl₂ and TBHP as oxidant did not show the low field signals observed with GtHNL-H96A (Figure 7A,B). Performing EPR spectroscopy in parallel mode enables the identification of integer spin states such as Mn(III) ($S = 2$) species (Figure 7C). A spectrum of GtHNL-H96A + TBHP showed the characteristic six-line pattern anticipated for Mn(III) at around 1300 G ($g = 5$). However, the control reaction using GtHNL-H96A without any oxidant showed the same pattern. We therefore attribute this signal to the spin forbidden $m_s = \pm 2$ transition of Mn(II) and not to Mn(III) (Figure 7C). Similar signals of Mn(II) in parallel mode EPR have been reported previously for the six-coordinated Mn in *Bacillus subtilis* oxalate decarboxylase.³¹ The signal of Mn(III) would be a very similar six-line pattern but centered at a lower field of circa 700 G, whereas the Mn(II) signal is centered around 1200 G. The ⁵⁵Mn ($I = 5/2$) hyperfine coupling constant $A(^{55}\text{Mn})$, which is the splitting of the six-line pattern, of GtHNL in parallel mode is 87 G (Figure 7C). A(⁵⁵Mn) value of 60 G has been reported for Mn(III) and 100 G for Mn(II) in oxalate decarboxylase.³¹ Simulation of the EPR spectra further supports the assignments (Figure S8).

The EPR studies did not demonstrate the expected oxidation of manganese from Mn(II) to Mn(III) but suggest the possibility of Mn(IV). Earlier UV assays for Mn(III)⁸ would actually support this, as both Mn(IV) and Mn(III) absorb at 265 nm and the former studies could not differentiate between the two ions.³² Organic radicals were not observed in any of the EPR spectra, which indicate that these may be too short lived and do not sufficiently accumulate in the samples. However, the best substrates for the oxidative cleavage bear a methyl group at the α position that might stabilize the more transient benzyl radical potentially formed after the addition of a *tert*-butylperoxy or similar radical. To probe whether the reaction proceeds via a radical mechanism, a radical scavenger was added. One equivalent of butyl hydroxytoluene (BHT) suppressed the reaction and resulted in only 2% yield of 4a (Figure S9). Thus, the formation of *tert*-butylperoxy radical is crucial for the enzymatic oxidative cleavage of styrene derivatives catalyzed by GtHNL-H96A.

The formation of radicals during the catalytic cycle of oxidative enzymatic alkene cleavage is not surprising and had been proposed earlier for Tm1459 (Scheme 3).⁹

Scheme 3. Manganese Catalyzed Oxidation of Alkenes Is Complex^a



^a(A) Oxygen and TBHP are required for the alkene cleavage catalyzed by GtHNL. (B) Haber–Weiss decomposition of peroxides leads to radical formation. (C) Possible oxygen and alkenes induced oxidation of Mn(II) to Mn(IV)^{34,35}

Overall, the oxidation chemistry catalyzed by Mn in metalloenzymes is complex.²² It is made even more complex by the fact that simple manganese compounds such as MnCO₃ and MnHPO₄ can also display superoxide dismutase activity.³³ Thus, the superoxide dismutases^{19,22} themselves and the ability of Mn(II) complexes to catalyze the essential superoxide (O_2^-) disproportionation with oxidation of Mn(II) to Mn(III)^{20,21,33} form one type of Mn catalysis.

Penta-coordinated Mn(II) complexes can activate molecular oxygen and have been reported to catalyze the oxidation of cyclohexene with epoxide, alcohol, and ketone as products; no alkene cleavage was observed.^{34,35} It was shown that the

Mn(II) complex is initially oxidized by either H_2O_2 or TBHP to produce a Mn(III) complex that is reduced back to Mn(II) by cyclohexene. The formation of Mn(III) and Mn(IV) complexes was confirmed for that conversion, as was the Haber–Weiss decomposition of peroxides (Scheme 3B,C).³⁵ Interestingly, the Mn catalyzed formation of epoxides has also been observed in biocatalysis and heterogeneous catalysis with oxidation reagents like TBHP and H_2O_2 .^{36–38}

The oxidative alkene cleavage utilizing oxygen as oxidant and manganese as active metal has been reported in an enzyme from *Trametes hirsuta*, unrelated to the cupins.^{39–41} The formation of alkoxy radicals with the incorporation of two different oxygen atoms from two different oxygen molecules for the alkene cleavage and the participation of Mn(III) were demonstrated in this very distinct mechanism.^{42,43} Recently, oxidative alkene cleavage activities via a peroxidase activity were observed for enzymes with a surface coordinated Mn. Here, H_2O_2 was the oxidizing reagent, and it was proposed that Mn(III) is an intermediate.^{44,45}

The oxidative alkene cleavage with TBHP, oxygen, and Mn(II) is thus a distinct activity (Scheme 3A). The *Tm1459* and *GtHNL* catalyzed oxidative alkene cleavage stands apart from all other Mn catalyzed alkene oxidation reactions. Although the otherwise common redox processes of Mn could not be observed here, the finding that one coordination site on Mn is sufficient to catalyze the oxidative cleavage of styrenes expands the range of cupins and other pentacoordinate metalloenzymes that can be employed in this reaction.

CONCLUSIONS

HNL catalyzed oxidative cleavage of styrene derivatives was observed. This is a completely different activity for HNLs that has not been previously reported. This oxidative cleavage of styrenes catalyzed by *GtHNL* is an existing enzymatic activity and was identified for HNLs by careful structural comparison with *Tm1459*. *GtHNL* was improved for this oxidative alkene cleavage reaction by rational protein engineering. The introduction of one amino acid substitution (H96A) in *GtHNL*-WT improved its catalytic activity. A 41% yield of acetophenone was reached after 20 h of reaction time by using *GtHNL*-H96A. The crystal structure of *GtHNL*-H96A shows that this modification generates accessibility of Mn similar to that in the active site of *Tm1459*. The enzyme catalyzed the oxidative cleavage of several styrene derivatives with yields ranging from 12 to 37% after 16 h of reaction time. *Tm1459*, on the other hand, showed a modest and unselective HNL activity.

Surprisingly, EPR studies did not provide direct evidence for the oxidation of Mn(II) to Mn(III). The reaction mechanism therefore remains unknown. However, a radical mechanism possibly involving Mn(IV) as the active species is plausible.

GtHNL-H96A conserved its natural HNL activity but lost its enantioselectivity (conv. = 47%, ee = 19%). Conversely, the variant *GtHNL*-V4 displayed poorer α -methyl styrene cleavage activity (acetophenone yield of 20.3% after 20 h of reaction time), but its natural HNL activity and enantioselectivity were not compromised (conv. = 98%, ee = 98%). Overall, this demonstrates that careful examination of structurally related enzymes can reveal unexpected activities, expanding the versatility of already known enzymes.

MATERIAL AND METHODS

Chemicals and Media. All chemicals were obtained from Sigma Aldrich (Schnelldorf, Germany) unless reported otherwise. The LB medium consisted of 1.00% (w/w) tryptone, 0.5% (w/w) yeast extract, and 1% NaCl and was autoclaved at 121 °C for 20 min. The terrific broth medium (TB medium) consisted of 1.20% (w/w) tryptone, 2.40% (w/w) yeast extract, 53 mM K_2HPO_4 , 16 mM KH_2PO_4 , and 4% (w/w) glycerol and was autoclaved at 121 °C for 20 min. The TB medium and potassium phosphate buffer components were autoclaved separately and mixed in a ratio of 9:1 under sterile conditions. Full details on how to perform all experiments for HNL activity can be found in the literature.³

Cloning and Heterologous Production of *GtHNL*-H96A and *GtHNL*-H96F. pET28a(+)-*GtHNL* expression plasmid containing the *GtHNL*-H96A gene codon optimized for *E. coli* was ordered from Bio Basic (Canada). Then, *E. coli* BL21(DE3) was transformed with the expression plasmid for the overexpression of *GtHNL*-H96A, and the plasmid was sequenced (Table S2). For the heterologous production of the enzyme, a preculture was prepared by inoculating one single colony of *E. coli* BL21(DE3)-pET28a*GtHNL*-H96A in 10 mL of lysogeny broth (LB) medium with kanamycin (50 $\mu\text{g}/\text{mL}$) and incubated overnight (New Brunswick Scientific Incubator Shaker Excella E24 Series) at 37 °C and 120 rpm. Subsequently, this preculture was used for the inoculation of 1 L of TB medium containing kanamycin (50 $\mu\text{g}/\text{mL}$) for the overexpression of *GtHNL*-H96A and incubated at 37 °C and 120 rpm. When the OD_{600} reached 0.6–0.8, the gene expression was induced by adding 1 mL of 0.1 M isopropyl β -D-thiogalactoside (IPTG) per liter of culture (0.1 mM IPTG final concentration). Moreover, 100–1000 μL of 1 M MnCl_2 was added per liter of culture at the induction time (0.1–1 mM Mn(II) final concentration), and cultivation was continued at 25 °C and 120 rpm for 20 h. Cells were harvested by centrifugation at 4 °C and 5000 rpm for 20 min (Sorvall RC6 centrifuge, Thermo Scientific). The supernatant was discarded, and the pellets were washed with 30 mL of 50 mM sodium phosphate buffer pH 7, frozen in liquid nitrogen, and stored at -80 °C. The same methodology was followed for the cloning and production of *GtHNL*-H96F using expression vector pET28a-*GtHNL*-H96F. A preculture of *E. coli* BL21-(DE3)-pET28a*GtHNL*-H96F (kanamycin 50 $\mu\text{g}/\text{mL}$) was prepared. The main culture was prepared by inoculating this preculture in 1 L of TB medium containing kanamycin (50 $\mu\text{g}/\text{mL}$) incubated at 37 °C and 120 rpm. The gene expression was induced at an OD_{600} of around 0.6–0.8 by adding 0.1 M of IPTG. At the same time, 100 μL of 1 M MnCl_2 was added to reach a final concentration of 0.1 mM MnCl_2 . The enzyme expression continued at 25 °C and 120 rpm for 20 h, and the isolation and purification were performed as explained earlier for the *GtHNL*-H96A.

Cloning and Heterologous Production of *GtHNL*-A40H/V42T/H96A/Q110H (*GtHNL*-4V). pET28a(+)-*GtHNL*-A40H/V42T/Q110H was used as template for the cloning of *GtHNL*-4V.³ The mutation H96A was introduced by overlap-extension PCR as described elsewhere.¹ The *GtHNL*-4V gene was cloned into pET28a expression vector using *Nco*I and *Hind*III restriction enzymes. The resulting pET28a-*GtHNL*-4V expression vector was cloned into *E. coli* TOP10 and sequenced to ensure the successful introduction of the H96A mutation (Table S3). Finally, the expression host *E.*

coli BL21(DE3) was transformed with pET28a(+)-GtHNL-4V for the overexpression of the GtHNL-4V enzyme. The heterologous production and harvesting of GtHNL-4V followed the same methodology described for GtHNL-H96A.

Purification of GtHNL-H96A, GtHNL-H96F, and GtHNL-4V. The pellets of GtHNL-H96A, GtHNL-H96F, and GtHNL-4V were resuspended in lysis buffer (50 mM sodium phosphate buffer + circa 50–70 mg DNase) pH 7 and lysed in a cell disruptor (Constant Systems Ltd., United Kingdom) at 1.37 kbar and 4 °C to avoid protein denaturation. The cell free extract (CFE) was collected as the supernatant after centrifugation at 4500g, 30 min, 4 °C; heated for 30 min at 65 °C; and centrifuged for 15 min at 4500g. The purified enzyme was obtained as the supernatant. For the EPR studies, GtHNL-H96A was further purified by anion exchange chromatography with a Q Sepharose Fast Flow column (HiTrap Q FF, 70 mL; GE Cytiva, Uppsala, Sweden).³ Bis-Tris buffer (50 mM) containing 30 mM NaCl pH 7.2 (buffer A) and Bis-Tris buffer (50 mM) containing 1 M NaCl pH 7.2 (buffer B) were used as binding and elution buffers, respectively. An isocratic step of 10% buffer B allowed the elution of pure GtHNL-H96A.

Alkene Cleavage Reactions under Optimal Conditions (Results in Table 1). The reactions were performed in a biphasic system in 2 mL plastic reaction tubes in accordance with an earlier report⁸ with slight modifications. Fifty microliters of 1 M substrate in ethyl acetate (3a–3h) (50 mM final concentration) and 50 μ L of 3 M *tert*-butyl hydroperoxide (TBHP) in *n*-decane (150 mM final concentration) were supplemented with 2 mg of GtHNL-H96A enzyme from the supernatant (see purification) and 50 mM sodium phosphate buffer pH 7. As result, the final reaction volume was 1 mL. The ratio of the organic/aqueous phase was 1:9. A thermomixer was used to shake the reaction tubes at 1000 rpm and to maintain 30 °C. Control reactions were performed with 0.5 mM MnCl₂. All the reactions were NOT quenched with sodium bisulfite at the end of the reaction time. MnCl₂ (0.5 mM) was used for the enzyme overexpression. The product was immediately extracted twice with ethyl acetate spiked with 10 mM *n*-dodecane as internal standard (1 \times 350 and 1 \times 500 μ L). The combined organic phases were dried using anhydrous MgSO₄ and injected for gas chromatography (GC) analysis.

Determination of *tert*-Butyl Hydroperoxide (TBHP). The concentration of TBHP was determined by iodometric titration with thiosulfate in accordance with the literature.⁴⁶ Briefly, 100 μ L of TBHP was dissolved in 10 mL acetic acid/chloroform (3:2), and nitrogen was sparged through the solution for 2 min to remove oxygen. Saturated potassium iodide solution (500 μ L) was added, and the head space was flushed with nitrogen for 1 min. Then, 15 mL of distilled water (sparged with nitrogen) and four drops of 1% starch (indicator) were added to produce a noticeable purple color. The sample was titrated with 0.01 N sodium thiosulfate until the purple color disappeared.

Inductively Couple Plasma Optical Emission Spectrometry (ICP-OES). Enzyme solution (0.5 mL) was digested in 4.5 mL milliQ water containing 1.5 mL 65% HNO₃ using a microwave (PRO, Anton Paar): ramp in 30 min to 200 °C, hold for 60 min at maximum power (1300 W), and cool down to 70 °C. Then, the samples were analyzed with ICP-OES (Perkin Elmer Optima 5300 DV). Wavelengths were as follows: 293.305, 294.920, 257.610, 259.372, and 260.568 nm.

Electron Paramagnetic Resonance (EPR) Studies. EPR spectra were recorded on a Bruker EMXplus spectrometer using a dual-mode resonator (Bruker ER 4116DM) with a helium-flow cryostat^{47,48} using the following EPR parameters: microwave frequency 9.624 GHz (perpendicular mode), 9.295 GHz (parallel mode); microwave power 20 mW; modulation frequency 100 kHz; modulation amplitude 10 G; and temperature 12.5 K. Perpendicular mode spectra were four times averaged; parallel mode spectra were nine times averaged. The protein concentration of the EPR samples was between 0.3 and 0.5 mM.

Gas Chromatography Analysis. Gas chromatography (GC) analysis was performed on a GC-2014 (Shimadzu) equipped with an AOC-20i auto injector by using N₂ as carrier gas, a cp wax S2 CB column (length: 50 m, I.D.: 0.53 mm, film thickness: 2 μ m, max temp: 250 °C), and an FID detector. The temperature profile is described as follows: first, 3 min at 100 °C; then, a gradient from 100 to 245 °C during 7.25 min at 20 °C/min; and finally, 1 min at 245 °C.

GtHNL-H96A Crystallization and Crystal Structure Determination. Crystals of GtHNL-H96A were initially obtained from a crystallization solution containing 30% PEG 2000 MME and 0.15 M KBr (QIAGEN-JCSG-Plus screening G10) using the vapor-diffusion method and the sitting drop technique. Further optimization of these conditions was pursued, and a suitable crystallization condition was identified (Additive Screen, Hampton Research B11) containing 0.1 M sodium citrate tribasic dihydrate as an additive. Crystals became visible after 4 days and were harvested using a crystal-direct harvester (<https://www.arinax.com/crystaldirect-automatic-protein-crystal-harvesting>)⁴⁹ after 8 days. X-ray diffraction data at 1.85 Å resolution were collected at the MX beamline P13 operated by EMBL at PETRA III, indexed and integrated with XDS,⁵⁰ and scaled with AIMLESS⁵¹ from the CCP4 program suite.⁵² Data collection statistics are given in Table S5. The structure of the apo-mutant enzyme was solved by the molecular replacement method using the program MOLREP⁵³ and the apo-form of the native enzyme (GtHNL) as a search model (PDB code: 4BIF).¹ Model building and refinement were performed with programs COOT⁵⁴ and REFMAC5⁵⁵ and/or PHENIX,⁵⁶ respectively, and checked periodically using the PDB-redo server (<https://pdb-redo.eu/>).⁵⁷ Thermal anisotropic parameterization (TLS) was also included in the refinement, with each monomeric subunit divided into different TLS groups, as suggested by TLS Motion Determination.^{58,59} During refinement, 5% of randomly selected observed reflections were kept aside for cross-validation. Model validation was done using MolProbity.⁶⁰ Structure refinement statistics are listed in Table S5. Figures were generated with PyMOL.⁶¹ All structural alignments between different crystal structures were done using the program GSAMT⁶² from the CCP4 program suite.

■ ASSOCIATED CONTENT

Supporting Information

The Supporting Information is available free of charge at <https://pubs.acs.org/doi/10.1021/acscatal.3c02249>.

Additional experimental data, including sequencing results and crystallographic data for the enzyme structure (PDF)

AUTHOR INFORMATION

Corresponding Author

Ulf Hanefeld – *Biokatalyse, Afdeling Biotechnologie, Technische Universiteit Delft, 2629 HZ Delft, Netherlands; orcid.org/0000-0002-4102-6165; Email: u.hanefeld@tudelft.nl*

Authors

José Coloma – *Biokatalyse, Afdeling Biotechnologie, Technische Universiteit Delft, 2629 HZ Delft, Netherlands; Universidad Laica Eloy Alfaro de Manabí, 130212 Manta, Ecuador*

Peter-Leon Hagedoorn – *Biokatalyse, Afdeling Biotechnologie, Technische Universiteit Delft, 2629 HZ Delft, Netherlands; orcid.org/0000-0001-6342-2022*

Isabel Bento – *EMBL Hamburg, 22607 Hamburg, Germany*

Complete contact information is available at:

<https://pubs.acs.org/10.1021/acscatal.3c02249>

Author Contributions

The manuscript was written through contributions of all authors. All authors have given approval to the final version of the manuscript.

Funding

This research was funded by the Secretary of Higher Education, Science, Technology and Innovation of Ecuador (Senescyt) and Universidad Laica Eloy Alfaro de Manabí (ULEAM).

Notes

The authors declare no competing financial interest.

ACKNOWLEDGMENTS

We acknowledge support at the SPC facility and at the EMBL beamlines at PETRA III storage ring, Hamburg. We acknowledge Cy M. Jeffries for performing the SEC-MALS experiments and for helpful discussions.

REFERENCES

- (1) Hajnal, I.; Lyskowski, A.; Hanefeld, U.; Gruber, K.; Schwab, H.; Steiner, K. Biochemical and structural characterization of a novel bacterial manganese-dependent hydroxynitrile lyase. *FEBS J.* **2013**, *280*, 5815–5828.
- (2) Wiedner, R.; Kothbauer, B.; Pavkov-Keller, T.; Gruber-Khadjawi, M.; Gruber, K.; Schwab, H.; Steiner, K. Improving the Properties of Bacterial R-Selective Hydroxynitrile Lyases for Industrial Applications. *ChemCatChem* **2015**, *7*, 325–332.
- (3) Coloma, J.; Guaiavarch, Y.; Hagedoorn, P.-L.; Hanefeld, U. Probing batch and continuous flow reactions in organic solvents: *Granulicella tundricola* hydroxynitrile lyase (GtHNL). *Catal. Sci. Technol.* **2020**, *10*, 3613–3621.
- (4) Vertregt, F.; Torrelo, G.; Trunk, S.; Wilsche, H.; Hagen, W. R.; Hanefeld, U.; Steiner, K. EPR Study of Substrate Binding to Mn(II) in Hydroxynitrile Lyase from *Granulicella tundricola*. *ACS Catal.* **2016**, *6*, 5081–5085.
- (5) Coloma, J.; Teeuwisse, L.; Afendi, M.; Hagedoorn, P.-L.; Hanefeld, U. Batch and Flow Nitroaldol Synthesis Catalysed by *Granulicella tundricola* Hydroxynitrile Lyase Immobilised on Celite R-633. *Catalysts* **2022**, *12*, 161.
- (6) Bekerle-Bogner, M.; Gruber-Khadjawi, M.; Wilsche, H.; Wiedner, R.; Schwab, H.; Steiner, K. (R)-selective nitroaldol reaction catalyzed by metal-dependent bacterial hydroxynitrile lyases. *ChemCatChem* **2016**, *8*, 2214–2216.
- (7) Jaroszewski, L.; Schwarzenbacher, R.; von Delft, F.; McMullan, D.; Brinen, L. S.; Canaves, J. M.; Dai, X.; Deacon, A. M.; DiDonato, M.; Elsiger, M.-A.; Eshagi, S.; Floyd, R.; Godzik, A.; Grittini, C.; Grzechnik, S. K.; Hampton, E.; Levin, I.; Karlak, C.; Klock, H. E.; Koesema, E.; Kovarik, J. S.; Kreusch, A.; Kuhn, P.; Lesley, S. A.; McPhillips, T. M.; Miller, M. D.; Morse, A.; Moy, K.; Ouyang, J.; Page, R.; Quijano, K.; Reyes, R.; Rezezadeh, F.; Robb, A.; Sims, E.; Spragg, G.; Stevens, R. C.; van den Bedem, H.; Velasquez, J.; Vincent, J.; Wang, X.; West, B.; Wolf, G.; Xu, Q.; Hodgson, K. O.; Wooley, J.; Wilson, I. A. Crystal structure of a novel manganese-containing cupin (TM1459) from *Thermotoga maritima* at 1.65 Å resolution. *Proteins: Struct., Funct., Bioinf.* **2004**, *56*, 611–614.
- (8) Hajnal, I.; Faber, K.; Schwab, H.; Hall, M.; Steiner, K. Oxidative Alkene Cleavage Catalysed by Manganese-Dependent Cupin TM1459 from *Thermotoga maritima*. *Adv. Synth. Catal.* **2015**, *357*, 3309–3316.
- (9) Fink, M.; Trunk, S.; Hall, M.; Schwab, H.; Steiner, K. Engineering of TM1459 from *Thermotoga maritima* for Increased Oxidative Alkene Cleavage Activity. *Front. Microbiol.* **2016**, *7*, 1511.
- (10) Dunwell, J. M.; Purvis, A.; Khuri, S. Cupins: the most functionally diverse protein superfamily? *Phytochemistry* **2004**, *65*, 7–17.
- (11) Dunwell, J. M. Cupins: A New Superfamily of Functionally Diverse Proteins that Include Germins and Plant Storage Proteins. *Biotechnol. Genet. Eng. Rev.* **1998**, *15*, 1–32.
- (12) Uberto, R.; Moomaw, E. W. Protein Similarity Networks Reveal Relationships among Sequence, Structure, and Function within the Cupin Superfamily. *PLoS One* **2013**, *8*, No. e74477.
- (13) Guzman, T.; Ribeiro de Souza, F. Z.; Carrilho, E.; Hanefeld, U. *Xylella fastidiosa* Esterase Rather than Hydroxynitrile Lyase. *ChemBioChem* **2015**, *16*, 625–630.
- (14) Dadashpour, M.; Asano, Y. Hydroxynitrile Lyases: Insights into Biochemistry, Discovery, and Engineering. *ACS Catal.* **2011**, *1*, 1121–1149.
- (15) Bracco, P.; Busch, H.; von Langermann, J.; Hanefeld, U. Enantioselective synthesis of cyanohydrins catalysed by hydroxynitrile lyases – a review. *Org. Biomol. Chem.* **2016**, *14*, 6375–6389.
- (16) Fujieda, N.; Ichihashi, H.; Yuasa, M.; Nishikawa, Y.; Kurisu, G.; Itoh, S. Cupin Variants as a Macromolecular Ligand Library for Stereoselective Michael Addition of Nitroalkanes. *Angew. Chem., Int. Ed.* **2020**, *59*, 7717–7720.
- (17) Grill, B.; Pavkov-Keller, T.; Grninger, C.; Darnhofer, B.; Gruber, K.; Hall, M.; Schwab, H.; Steiner, K. Engineering TM1459 for Stabilisation against Inactivation by Amino Acid Oxidation. *Chem. Ing. Tech.* **2023**, *95*, 596–606.
- (18) Matsumoto, R.; Yoshioka, S.; Yuasa, M.; Morita, Y.; Kurisu, G.; Fujieda, N. An artificial metallozyme with pliable 2-His-1-carboxylate facial triad for stereoselective Michael addition. *Chem. Sci.* **2023**, *14*, 3932–3937.
- (19) Rice, D. B.; Massie, A. A.; Jackson, T. A. Manganese–Oxygen Intermediates in O–O Bond Activation and Hydrogen-Atom Transfer Reactions. *Acc. Chem. Res.* **2017**, *50*, 2706–2717.
- (20) Kenkel, I.; Franke, A.; Dürr, M.; Zahl, A.; Dücker-Benfer, C.; Langer, J.; Filipović, M. R.; Yu, M.; Puchta, R.; Fiedler, S. R.; Shores, M. P.; Goldsmith, C. R.; Ivanović-Burmazović, I. Switching between Inner- and Outer-Sphere PCET Mechanisms of Small-Molecule Activation: Superoxide Dismutation and Oxygen/Superoxide Reduction Reactivity Deriving from the Same Manganese Complex. *J. Am. Chem. Soc.* **2017**, *139*, 1472–1484.
- (21) Signorella, S.; Palopoli, C.; Ledesma, G. Rationally designed mimics of antioxidant manganoenzymes: Role of structural features in the quest for catalysts with catalase and superoxide dismutase activity. *Coord. Chem. Rev.* **2018**, *365*, 75–102.
- (22) Christianson, D. W. Structural chemistry and biology of manganese metalloenzymes. *Prog. Biophys. Mol. Biol.* **1997**, *67*, 217–252.
- (23) Banerjee, A.; Tolla, A. S.; Stjepanovic, S.; Sevilla, M. D.; Goodsell, J. L.; Angerhofer, A.; Brennessel, W. W.; Loloe, R.; Chavez, F. A. Structural, spectroscopic, electrochemical, and magnetic properties for manganese(II) triazamacrocyclic complexes. *Inorg. Chim. Acta* **2019**, *486*, 546–555.

- (24) Jones, B. J.; Evans, R. L., III; Mylrea, N. J.; Chaudhury, D.; Luo, C.; Guan, B.; Pierce, C. T.; Gordon, W. R.; Wilmot, C. M.; Kazlauskas, R. J. Larger active site in an ancestral hydroxynitrile lyases increases catalytically promiscuous esterase activity. *PLoS One* **2020**, *15*, No. e0235341.
- (25) Hiatt, R.; Clipsham, J.; Visser, T. The induced decomposition of tert-butyl hydroperoxide. *Can. J. Chem.* **1964**, *42*, 2754–2757.
- (26) Qi, L.; Qi, X.; Wang, L.; Feng, L.; Lu, S. Decomposition of tert-butyl hydroperoxide into tert-butyl alcohol and O₂ catalyzed by birnessite-type manganese oxides: Kinetics and activity. *Catal. Commun.* **2014**, *49*, 6–9.
- (27) Liu, H.; Gu, L.; Zhu, P.; Liu, Z.; Zhou, B. Evaluation on thermal hazard of ter-butyl hydroperoxide by using accelerating rate calorimeter. *Procedia Eng.* **2012**, *45*, 574–579.
- (28) Good, N. E.; Winget, G. D.; Winter, W.; Connolly, T. N.; Isawa, S.; Singh, R. M. M. Hydrogen Ion Buffers for Biological Research. *Biochemistry* **1966**, *5*, 467–477.
- (29) Scheller, K. H.; Abel, T. H. J.; Polanyi, P. E.; Wenk, P. K.; Fischer, B. E.; Sigel, H. Metal ion / buffer interactions. *Eur. J. Biochem.* **1980**, *107*, 455–466.
- (30) Guo, A. C.; Jewison, T.; Wilson, M.; Liu, Y.; Knox, C.; Djoumbou, Y.; Lo, P.; Mandal, R.; Krishnamurthy, R.; Wishart, D. S. ECMD: the *E. coli* Metabolome Database. *Nucleic Acids Res.* **2013**, *41*, D625–D630.
- (31) Zhu, W.; Wilcoxon, J.; Britt, R. D.; Richards, N. G. J. Formation of hexacoordinate Mn(III) in *Bacillus subtilis* Oxalate Decarboxylase requires catalytic turnover. *Biochemistry* **2016**, *55*, 429–434.
- (32) Jee, J.-E.; Pestovsky, O.; Bakac, A. Preparation and characterization of manganese(IV) in aqueous acetic acid. *Dalton Trans.* **2010**, *39*, 11636–11642.
- (33) Barnese, K.; Gralla, E. B.; Valentine, J. S.; Cabelli, D. E. Biologically relevant mechanism for catalytic superoxide removal by simple manganese compounds. *Proc. Natl. Acad. Sci. U. S. A.* **2012**, *109*, 6892–6897.
- (34) Rydel-Ciszek, K.; Charczuk, M.; Paczeński, T.; Chmielarz, P. Manganese(II) complexes with Bn-tpen as powerful catalysts of cyclohexene oxidation. *Chem. Pap.* **2017**, *71*, 2085–2093.
- (35) Luts, T.; Frank, R.; Suprun, W.; Fritzsche, S.; Hey-Hawkins, E.; Papp, H. Epoxidation of olefins catalyzed by novel Mn(III) and Mo(IV)-Salen complexes immobilized on mesoporous silica gel Part II: Study of the catalytic epoxidation of olefins. *J. Mol. Catal. A: Chem.* **2007**, *273*, 250–258.
- (36) Okrasa, K.; Kazlauskas, R. J. Manganese-Substituted Carbonic Anhydrase as a New Peroxidase. *Chem. – Eur. J.* **2006**, *12*, 1587–1596.
- (37) Tušar, N. N.; Jank, S.; Gläser, R. Manganese-Containing Porous Silicates: Synthesis, Structural Properties and Catalytic Applications. *ChemCatChem* **2011**, *3*, 254–269.
- (38) Ramanathan, A.; Archipov, T.; Maheswari, R.; Hanefeld, U.; Roduner, E.; Gläser, R. Synthesis, Characterization and Catalytic Properties of the Novel Manganese-Containing Amorphous Mesoporous Material MnTUD-1. *J. Phys. Chem. C* **2008**, *112*, 7468–7476.
- (39) Mang, H.; Gross, J.; Lara, M.; Goessler, C.; Schoemaker, H. E.; Guebitz, G. M.; Kroutil, W. Biocatalytic Single-Step Alkene Cleavage from Aryl Alkenes: An Enzymatic Equivalent to Reductive Ozonization. *Angew. Chem., Int. Ed.* **2006**, *45*, S201–S203.
- (40) Paul, C. E.; Rajagopalan, A.; Lavandera, I.; Gotor-Fernández, V.; Kroutil, W.; Gotor, V. Expanding the regioselective enzymatic repertoire: oxidative mono-cleavage of dialkenes catalyzed by *Trametes hirsuta*. *Chem. Commun.* **2012**, *48*, 3303–3305.
- (41) Rajagopalan, A.; Lara, M.; Kroutil, W. Oxidative Alkene Cleavage by Chemical and Enzymatic Methods. *Adv. Synth. Catal.* **2013**, *355*, 3321–3335.
- (42) Lara, M.; Mutti, F. G.; Glueck, S. M.; Kroutil, W. Oxidative Enzymatic Alkene Cleavage: Indications for a Nonclassical Enzyme Mechanism. *J. Am. Chem. Soc.* **2009**, *131*, S368–S369.
- (43) Rajagopalan, A.; Schober, M.; Emmerstorfer, A.; Hammerer, L.; Migglautsch, A.; Seisser, B.; Glueck, S. M.; Niehaus, F.; Eck, J.; Pichler, H.; Gruber, K.; Kroutil, W. Enzymatic aerobic alkene cleavage catalyzed by a Mn³⁺-dependent Proteinase A homologue. *ChemBioChem* **2013**, *14*, 2427–2430.
- (44) Krahe, N.-K.; Berger, R. G.; Ersoy, F. A DyP-Type Peroxidase of *Pleurotus sapidus* with Alkene Cleaving Activity. *Molecules* **2020**, *25*, 1536.
- (45) Krahe, N.-K.; Berger, R. G.; Witt, M.; Zorn, H.; Omarini, A. B.; Ersoy, F. Monokaryotic *Pleurotus sapidus* Strains with Intraspecific Variability of an Alkene Cleaving DyP-Type Peroxidase Activity as a Result of Gene Mutation and Differential Gene Expression. *Int. J. Mol. Sci.* **2021**, *22*, 1363.
- (46) AOAC official method 41.1.16. Peroxide value of oils and fats. Official method of Analysis of AOAC International, 16th edn., AOAC International Gaithersburg, 1997, DOI: 10.1093/9780197610145.001.0001.
- (47) Salmeen, I.; Palmer, G. Electron Paramagnetic Resonance of Beef-Heart Ferricytochrome C. *J. Chem. Phys.* **1968**, *48*, 2049–2052.
- (48) Lundin, A.; Aasa, R. A Simple Device to Maintain Temperatures in the Range 4.2–100 K for EPR Measurements. *J. Magn. Reson.* **1972**, *8*, 70–73.
- (49) Felisaz, F.; Sinoir, J.; Papp, G.; Pica, A.; Bowler, M. W.; Murphy, P.; Hoffmann, G.; Zander, U.; Lopez-Marrero, M.; Janocha, R.; Giraud, T.; Svensson, O.; Popov, S.; Leonard, G.; Mueller-Dieckmann, C.; Márquez, J. A.; McCarthy, A. A.; Cipriani, F. CrystalDirect-To-Beam: Opening the shortest path from crystal to data. *AIP Conf. Proc.* **2019**, 2054, No. 050009.
- (50) Kabsch, W. XDS. *Acta Crystallogr., Sect. D: Biol. Crystallogr.* **2010**, *66*, 125–132.
- (51) Evans, P. R. An introduction to data reduction: space-group determination, scaling and intensity statistics. *Acta Crystallogr., Sect. D: Biol. Crystallogr.* **2011**, *67*, 282–292.
- (52) Collaborative. The CCP4 suite: programs for protein crystallography. *Acta Crystallogr., Sect. D: Biol. Crystallogr.* **1994**, *50*, 760–763.
- (53) Vagin, A.; Teplyakov, A. MOLREP: an automated program for molecular replacement. *J. Appl. Crystallogr.* **1997**, *30*, 1022–1025.
- (54) Emsley, P.; Lohkamp, B.; Scott, W. G.; Cowtan, K. Features and development of Coot. *Acta Crystallogr., Sect. D: Biol. Crystallogr.* **2010**, *66*, 486–501.
- (55) Murshudov, G. N.; Skubák, P.; Lebedev, A. A.; Pannu, N. S.; Steiner, R. A.; Nicholls, R. A.; Winn, M. D.; Long, F.; Vagin, A. A. REFMAC5 for the refinement of macromolecular crystal structures. *Acta Crystallogr., Sect. D: Biol. Crystallogr.* **2011**, *67*, 355–367.
- (56) Adams, P. D.; Afonine, P. V.; Bunkóczi, G.; Chen, V. B.; Davis, I. W.; Echols, N.; Headd, J. J.; Hung, L. W.; Kapral, G. J.; Grosse-Kunstleve, R. W.; McCoy, A. J.; Moriarty, N. W.; Oeffner, R.; Read, R. J.; Richardson, D. C.; Richardson, J. S.; Terwilliger, T. C.; Zwart, P. H. PHENIX: a comprehensive Python-based system for macromolecular structure solution. *Acta Crystallogr., Sect. D: Biol. Crystallogr.* **2010**, *66*, 213–221.
- (57) Joosten, R. P.; Long, F.; Murshudov, G. N.; Perrakis, A. The PDB_REDO server for macromolecular structure model optimization. *IUCrJ* **2014**, *1*, 213–220.
- (58) Painter, J.; Merritt, E. A. Optimal description of a protein structure in terms of multiple groups undergoing TLS motion. *Acta Crystallogr., Sect. D: Biol. Crystallogr.* **2006**, *62*, 439–450.
- (59) Painter, J.; Merritt, E. A. TLSMD web server for the generation of multi-group TLS models. *J. Appl. Cryst.* **2006**, *39*, 109–111.
- (60) Williams, C. J.; Headd, J. J.; Moriarty, N. W.; Prisant, M. G.; Videau, L. L.; Deis, L. N.; Verma, V.; Keedy, D. A.; Hintze, B. J.; Chen, V. B.; Jain, S.; Lewis, S. M.; Arendall, W. B., III; Snoeyink, J.; Adams, P. D.; Lovell, S. C.; Richardson, J. S.; Richardson, D. C. MolProbity: More and better reference data for improved all-atom structure validation. *Protein Sci.* **2018**, *27*, 293–315.
- (61) Schrödinger, L.; DeLano, W. **2020**. PyMOL, Available at: <https://www.pymol.org/pymol.html> visited on 06/14/2023.
- (62) Krissinel, E. Enhanced Fold Recognition using Efficient Short Fragment Clustering. *J. Mol. Biochem.* **2012**, *1*, 76–85.